IEEE Access
Multidisciplinary | Rapid Review | Open Access Journal

Received 19 May 2023, accepted 2 June 2023, date of publication 7 June 2023, date of current version 12 June 2023.

Digital Object Identifier 10.1109/ACCESS.2023.3283569

RESEARCH ARTICLE

Experimental Demonstration of Wave Source Location Estimation Method for Spectrum Sharing in 28-GHz-Band 5G System

HIROFUMI SUGANUMA[1], (Member, IEEE), TSUTOMU MITSUI[1], AND TAKAHIRO MATSUDA[2], (Member, IEEE)

[1]Test and Measurement Company, Anritsu Corporation, Atsugi-shi, Kanagawa 243-8555, Japan
[2]Graduate School of Systems Design, Tokyo Metropolitan University, Hino-shi, Tokyo 191-0065, Japan

Corresponding author: Hirofumi Suganuma (Hirofumi.Suganuma@anritsu.com)

ABSTRACT This paper experimentally investigates a direction of arrival (DOA)-based wave source location estimation method for spectrum sharing in millimeter-wave band local and private fifth-generation (5G) mobile communication systems. In the DOA-based wave source location estimation, it is important to extract a line-of-sight (LOS) component from the received signals. Considering that in 5G systems, synchronization signal / physical broadcast channel (SS/PBCH) blocks are transmitted with beam-sweeping for initial access, our measurement system performs the DOA estimation based on the maximum-power block where the LOS component seems to be dominant. In the DOA estimation, taking advantage of the sparsity of the propagation channels in both angular space and delay time domains, our measurement system adopts the compressed sensing (CS)-based approach. As for the measurement antenna, a directional pattern is employed, which enables the estimation with only four antenna elements. We experimentally demonstrate the performance of the wave source location estimation in an outdoor environment using a commercial 28 GHz-band 5G base station (BS). Experimental results show that our measurement system achieves a location estimation error of 5.8 m based on 20 measurements.

INDEX TERMS Wave source location estimation, fifth-generation mobile communication systems (5G), millimeter-wave, direction of arrival (DOA) estimation, compressed sensing (CS).

I. INTRODUCTION

The number of global mobile subscriptions is estimated to reach 9.2 billion by 2028 [1], and the demands for mobile network services are becoming more stringent and diverse [2]. Fifth-generation (5G) mobile communication systems offer enhanced performance and functionality, such as enhanced mobile broadband (eMBB), ultra-reliable and low-latency communications (URLLC), and massive machine type communications (mMTC) [3], [4]. As a result, 5G networks have the potential to support a variety of application scenarios through a unified air interface [4].

However, public 5G networks provided by mobile network operators are designed based on the common needs of their subscribers in pursuit of revenue, and therefore do not meet the needs of all users in terms of the coverage, capacity, security, and customizability [5], [6]. In this context, local and private 5G networks, also referred to as non-public networks by the 3rd Generation Partnership Project (3GPP), are attracting attention [5], [6], [7], [8], [9]. This is because such networks can be configured for specific use cases, such as factories, airports, hospitals, and campus environments [6].

Local and private 5G networks are assumed to be deployed in specific areas. To efficiently reuse limited spectrum resources among different networks, spectrum sharing techniques have been investigated [10], [11], [12], [13], [14], [15], [16], [17]. In [10], a 5G heterogeneous network consisting of multiple primary networks with channels available to secondary users was studied, and a network selection and channel allocation method was proposed to minimize the

The associate editor coordinating the review of this manuscript and approving it for publication was Sotirios Goudos.

interference to primary networks and costs paid by secondary users. In [11], since cognitive radio devices consume more energy to perform dedicated functions, such as spectrum sensing and sharing, a cooperative mechanism for both wireless energy harvesting and spectrum sharing was proposed. In [12], spectrum sharing between radar and communication systems was investigated, and an interference mitigation method enjoying the advantage of null-space projection based on overlapped virtual subarrays was proposed. Furthermore, in the spectrum sharing, a secondary system does not interfere with a primary system in principle, and hence it is necessary to obtain the radio wave source location information of the primary system for interference coordination. However, the location information may not be available or disclosed for temporary or license-exempt system, because it is not recorded in the database [18]. Thus, several approaches for wave source location estimation, such as received signal strength (RSS) [19], [20], [21], [22], time difference of arrival (TDOA) [23], [24], and direction of arrival (DOA) [18], [25], [26], [27], [28], [29], [30], [31], have been studied. From a practical point of view, the DOA-based approach is considered as a promising technique that realizes the high estimation accuracy [32]. The performance of the DOA-based wave source location estimation has been experimentally investigated in the sub-6 GHz band [27], [28], [29], [30] and in the millimeter-wave band [18], [31]. The authors in [18] and [31] focused on fixed wireless systems and proposed a method for estimating parameters including wave source location. However, to the best of our knowledge, no existing literature has designed the wave source location estimation for actual 5G base stations (BSs) in the millimeter-wave band.

In this paper, we experimentally investigate a wave source location estimation method for the spectrum sharing in the millimeter-wave band 5G system. In the DOA-based wave source location estimation, it is important to extract the line-of-sight (LOS) component from received signals [25], [31]. In particular, a beamforming technique is generally adopted as a countermeasure against large pathloss in millimeter-wave band 5G systems [4], [33], [34], and even if the LOS between a transmitter and receiver is maintained, the non-line-of-sight (NLOS) component can be dominant in the case where the transmit beam is not directed to the receiver. Therefore, considering that the synchronization signal / physical broadcast channel (SS/PBCH) blocks used for the initial access in 5G systems are transmitted with beam-sweeping [35], [36], [37], our measurement system performs the DOA estimation by using the maximum-power block where the LOS component appears to be dominant. The DOA estimation is carried out based on the compressed sensing (CS) technique, which enables high-resolution estimation from a single snapshot [15], [38], [39], [40], [41], [42], [43], and exploits the sparsity of the propagation channels in both angular space and delay time domains [42], [43] owing to the broadband and directional 5G signals [4]. As for the measurement antenna in our system, a directional pattern is adopted, which makes it possible to estimate the DOA with only four antenna elements [41]. Moreover, we present experimental results of the wave source location estimation method in an outdoor environment using a commercial 28 GHz-band 5G BS.

The remainder of the paper is organized as follows. Section II provides an overview of the existing works related to the wave source location estimation. Section III describes the system concept and operating principle of the wave source location estimation method for the millimeter-wave band 5G system. Section IV presents the experimental results and their discussion. Finally, the conclusions are drawn in Section V.

Notations: $(\cdot)^*$, $(\cdot)^{\mathsf{T}}$, and $(\cdot)^{\mathsf{H}}$ denote the complex conjugate, transpose, and conjugate transpose, respectively. $[\cdot]_{i,j}$, $\mathrm{vec}(\cdot)$, and $\lambda_{\max}(\cdot)$ are the (i, j) element, vectorization operator, and maximum eigenvalue, respectively. $\otimes$ denotes the Kronecker product.

II. RELATED WORKS

Table 1 lists the existing studies on the wave source location estimation. The source location estimation method is classified into three approaches: RSS [19], [20], [21], [22], TDOA [23], [24], and DOA [18], [25], [26], [27], [28], [29], [30], [31]. A comprehensive performance comparison of these approaches in millimeter-wave band wireless systems was presented in [32].

The RSS-based approach [19], [20], [21], [22] exploits the fact that the signal strength attenuates depending on the propagation distance, and can be easily implemented without any additional special measurement functions. In [19], the user location was estimated from the uplink RSS information without prior knowledge of the transmit power and pathloss exponent in distributed massive MIMO environments. However, the log-distance pathloss model was assumed as the radio propagation model; the applicability of this approach to realistic propagation environments is open to discussion. In [20], such a concern with radio propagation modeling was alleviated by calculating the power gravity point from sensor locations and RSSs, and the locations of multiple wave sources were estimated owing to a region division technique. The effectiveness of this method was experimentally demonstrated using a commercial 2 GHz-band Long Term Evolution (LTE) BS. However, in this method, the localization error can approach half the distance between adjacent sensors, and to achieve high-precision localization, it is necessary to place sensors at a high density. In [21], locations and transmit powers of multiple wave sources were estimated by applying deep learning to a gray-scale image obtained from RSSs and sensor locations. In [22], an RSS fingerprinting-based localization method using deep learning was proposed, which improved the localization accuracy by employing channel set splitting and adversarial training for the challenges posed by multi-channel RSS measurements and device heterogeneity. However, in practice, the wave sources are assumed to be in different locations; therefore, such deep learning-based approaches [21], [22] may have difficulty in performing the

TABLE 1. Overview of Existing Studies on Wave Source Location Estimation.

Ref.	Approach method	Features	Verification methodology
[19]	Distributed massive MIMO localization using RSS	Can estimate source location without knowledge of transmit power and pathloss exponent	Computer simulation
[20]	Region division and RSS-based gravity point calculation	Can estimate locations of multiple sources	Computer simulation and experimental demonstration
[21]	Application of deep learning to gray-scale image obtained from RSSs and sensor locations	Can estimate locations and transmit powers of multiple sources	Computer simulation and experimental demonstration
[22]	RSS fingerprinting-based localization using deep learning	Channel set splitting and adversarial training for multichannel RSS measurements and device heterogeneity	Theoretical analysis and experimental demonstration
[23]	TDOA-based localization with greedy algorithm-like sensor selection	High robustness against TDOA measurement error and low computational complexity	Computer simulation
[24]	TDOA-based localization with reference BS selection using machine learning	High accurate localization in complex wireless environments, such as IIoT scenarios	Computer simulation
[25]	DOA- and TOA-based localization assisted by beamforming	High accurate localization by extracting LOS component using beamforming	Computer simulation
[26]	DOA- and TOA-based localization by single BS	Can estimate locations of transmitter and reflectors, simultaneously	Computer simulation
[27]	Incremental localization using DOA based on MUSIC	Measurement by UAV and spark noise reduction in DOA estimates	Experimental demonstration
[28]	DOA-based localization exploiting common sparsity property of massive MIMO channels	Achieve centimeter-level precision estimation in the presence of dense multipath	Computer simulation and experimental demonstration
[29], [30]	CS-based localization using DOA in UAV environments	Indicate potential of UAV-based localization employing array antenna with few elements, e.g., four or six elements	Computer simulation and experimental demonstration
[18]	ML-based estimation using DOA, Rx power, and map database	Can estimate Tx location, orientation, power, and antenna beamwidth, simultaneously	Experimental demonstration
[32]	Localization based on RSS, TDOA, or DOA	Comprehensive performance comparison of localization approaches in millimeter-wave band	Computer simulation

training phase under any radio propagation environment [18]. In addition, the RSS-based approach [19], [20], [21], [22] is highly dependent on the radio propagation behavior, which makes it difficult to apply to millimeter-wave band systems where the channel gain is significantly changed by beamforming.

The TDOA-based approach [23], [24] utilizes the propagation delay, which also depends on the propagation distance. In [23], a TDOA-based localization method with greedy algorithm-like sensor selection was proposed, which achieved the high robustness against TDOA measurement error and low computational complexity. In [24], a reference BS selection method based on machine learning was proposed, which led to the highly accurate localization even in complex wireless environments, such as industrial internet of things (IIoT) scenarios. However, these TDOA-based approaches require time synchronization among multiple measurement points.

In a practical sense, the DOA-based approach [18], [25], [26], [27], [28], [29], [30], [31] can be seen as a promising technique that realizes the high accuracy estimation [32]. In [25], the user location was estimated based on both DOA and time of arrival (TOA), and the LOS component was obtained by beamforming to improve the estimation accuracy. In [26], the locations of the transmitter and reflectors were estimated simultaneously based on both DOA and TOA. However, in these approaches [25], [26], time synchronization between the transmitter and receiver is required to measure the TOA; thus, they are not suitable for the wave source localization for the spectrum sharing. In [27], experimental evaluations of wave source localization using an unmanned aerial vehicle (UAV) were performed at the 1.5 GHz band, where multiple signal classification (MUSIC) was adopted for DOA estimation. In [28], a DOA-based localization method that exploits the common sparsity property of massive MIMO channels was proposed, and its effectiveness was experimentally demonstrated using a 6 GHz-band 5G testing BS. However, these approaches [27], [28] require multiple incoherent signals for DOA estimation; in actual communication scenarios, the DOA estimation tends to fail due to coherent signals [44]. In [29] and [30], the adoption of the CS-based technique, which enables the high-resolution DOA estimation by a single snapshot [15], [38], [39], [40], [41], [42], [43], was investigated in UAV environments, and the potential of UAV-based localization using an array antenna with few elements, e.g., four or six elements, was indicated. In contrast to [27], [28], and [30], a method for estimating wave source parameters, such as location, orientation, transmit power, and antenna beamwidth, was proposed for fixed wireless systems and experimentally demonstrated at the 26 GHz band in [18].

Compared with the existing works, an objective of this paper is to experimentally investigate the wave source location estimation for the spectrum sharing in the

millimeter-wave band 5G system. The features of our work are as follows:

- To improve the estimation accuracy, the LOS component extraction is performed. Compared with [25], our approach takes advantage of the fact that SS/PBCH blocks used for the initial access in 5G systems are transmitted with beam-sweeping.
- The CS-based DOA estimation is performed exploiting the sparsity of propagation channels in both angular space and delay time domains owing to the broadband and directional 5G signals [4]. This approach can further extract the LOS component, which is inspired by the existing studies on the joint DOA and time of arrival (TOA) estimation method for wireless communication systems [42] and radar systems [43]. In [42] and [43], the omni-directional antenna elements were assumed, whereas we have so far theoretically investigated the accuracy improvement of the CS-based DOA estimation employing directional antenna elements [41]. Based on our previous study [41], the directional antenna elements are adopted herein, which enables us to estimate the DOA with only four elements.
- In the CS-based approach, the property of the sensing matrix determines the reconstruction accuracy of sparse signals, and smaller correlation coefficients calculated from its matrix provide the better reconstruction performance [41], [45]. Thus, such correlation coefficients are analyzed in the DOA and delay domains, respectively. In the DOA domain, our correlation analysis verifies that the experimental antenna with directional elements reduces the correlation compared with the omni-directional antenna. In the delay domain, the configuration of the signals that should be used for the DOA estimation is clarified.
- The performance of the wave source location estimation is experimentally demonstrated in an outdoor environment using a commercial 28 GHz-band 5G BS. In particular, the effect of the difference in the transmit beams on DOA estimation, which is essential for the wave source localization, is clarified.

III. WAVE SOURCE LOCATION ESTIMATION METHOD FOR MILLIMETER-WAVE BAND 5G SYSTEM

A. SYSTEM CONCEPT

Fig. 1 illustrates the concept of the DOA-based wave source location estimation, where K is the number of Rx points and ϕ_k $(k = 1, 2, \cdots, K)$ is the DOA at Rx point #k. As shown in Fig. 1, the DOAs at two or more Rx points are estimated using the array antenna, and then the radio wave source, or Tx location, is identified based on such DOAs and Rx locations. However, this approach assumes that the geographical relationship between the Tx and Rx can be obtained from a direct wave, and suffers from an inherent problem that the accuracy of the location estimation is significantly degraded in NLOS environments [31]. This problem cannot

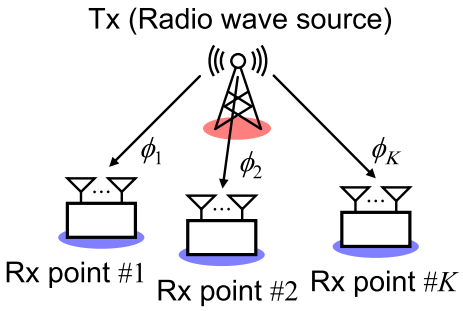

FIGURE 1. Concept of DOA-based wave source location estimation.

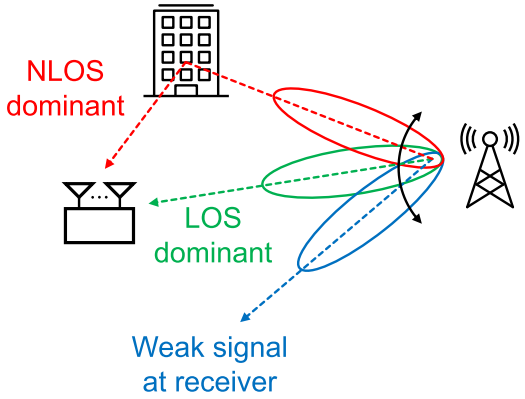

FIGURE 2. Effect of beamforming on wave source location estimation in millimeter-wave band.

be ignored even in millimeter-wave band 5G systems using beamforming technology.

Fig. 2 shows the effect of beamforming on the DOA-based wave source location estimation. Even if the LOS between the Tx and Rx is maintained, the NLOS component can be dominant due to a reflected wave in the case where the transmit beam is not aimed at the Rx but at other objects, such as buildings. Furthermore, in the worst case, both direct and reflected waves fail to reach the Rx, making it difficult to even estimate the DOA.

Therefore, our measurement system extracts the LOS component from the received signals to improve the accuracy of the DOA-based wave source location estimation. Fig. 3 shows the overall configuration of the wave source location estimation method for the millimeter-wave band 5G system. In the 5G system, SS/PBCH blocks are transmitted with beam-sweeping for the initial access [35], [36], [37]. Here, in relatively high-power SS/PBCH blocks, the LOS component is considered to be dominant, and hence the DOA estimation is performed based on the maximum-power SS/PBCH block. In the DOA estimation, taking advantage of the sparsity of the propagation channels in both angular space and delay time domains, our measurement system adopts the CS-based approach, which enables high-resolution estimation by a single snapshot [15], [38], [39], [40], [41], [42], [43]. Since the signal with the highest power in the DOA and delay time domains is the LOS component, the DOA corresponding to

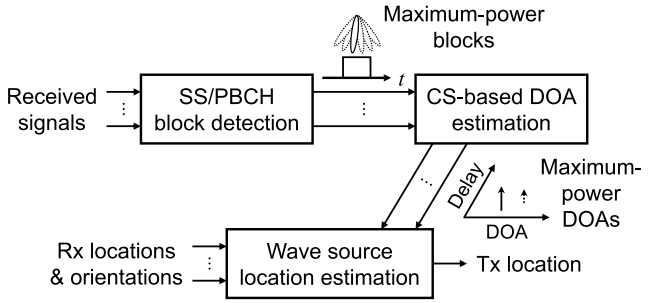

FIGURE 3. Overall configuration of DOA-based wave source location estimation method for millimeter-wave band 5G system.

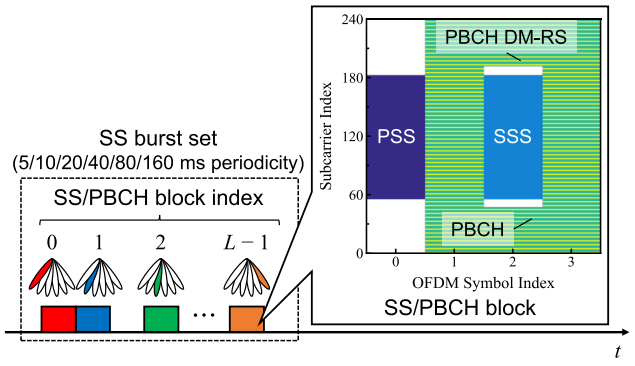

FIGURE 4. Relationship between SS/PBCH blocks and transmit beams in 5G systems.

such a signal is used for the wave source location estimation, as well as the Rx location and orientation obtained by a global positioning system (GPS) compass.

B. SS/PBCH BLOCK DETECTION

Fig. 4 illustrates the relationship between SS/PBCH blocks and transmit beams. In 5G systems, the BS transmits SS/PBCH blocks containing synchronization signals and broadcast information for the initial access [35], [36], [37]. Each SS/PBCH block consists of four orthogonal frequency-division multiplexing (OFDM) symbols, including the primary synchronization signal (PSS), secondary synchronization signal (SSS), physical broadcast channel (PBCH), and demodulation reference signal (DM-RS). By synchronizing and demodulating these signals, the physical-layer cell identity, SS/PBCH block index, system frame number, and other information can be retrieved. In addition, a synchronization signal (SS) burst set is composed of L (≤ 64) SS/PBCH blocks for BS beam-sweeping transmission and is transmitted periodically, e.g., every 20 ms [37].

In our measurement system, since the LOS component appears to be dominant, the SS/PBCH block with the maximum desired power is selected and used for subsequent processing, such as the CS-based DOA estimation and wave source location estimation. Note that the SS reference signal received power (SS-RSRP), which is defined as the average power of the resource elements that carry the SSS [46], can be used as a measure of the desired power.

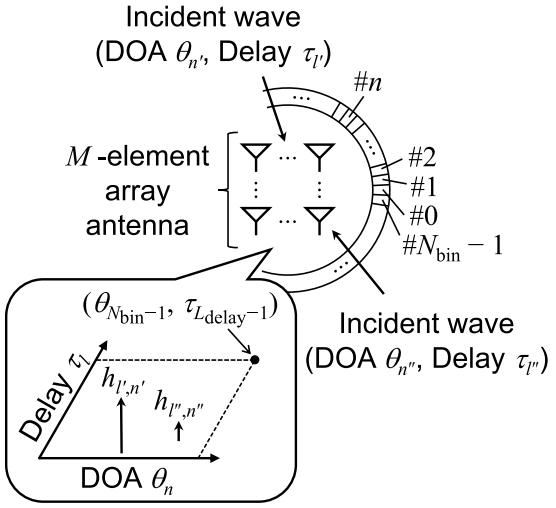

FIGURE 5. Concept of CS-based DOA estimation.

C. CS-BASED DOA ESTIMATION

Fig. 5 illustrates the concept of the CS-based DOA estimation. As shown in Fig. 5, the angular space is divided into N_{bin} small regions that is called bins [39], [40], [41], [42]. An OFDM signal arrives at an M-element array antenna through the bin of angle θ_n ($n = 0, 1, \cdots, N_{\text{bin}} - 1$), which is delayed by τ_l ($l = 0, 1, \cdots, L_{\text{delay}} - 1$). The CS-based DOA estimation exploits the sparsity of propagation channels in both angular space and delay time domains [42], [43].

Here, we apply the CS-based DOA estimation to N_{RS} reference signals (RSs) contained in the SS/PBCH block. The frequency-domain OFDM signal through the finite impulse response (FIR) channel is expressed as $\mathbf{XFh}_n$ [39], [47], where $\mathbf{X} = \text{diag}\{X_0, X_1, \cdots, X_{N_{\text{RS}}-1}\} \in \mathbb{C}^{N_{\text{RS}} \times N_{\text{RS}}}$, $\mathbf{F} = [f_{p,l}] \in \mathbb{C}^{N_{\text{RS}} \times L_{\text{delay}}}$, and $\mathbf{h}_n = [h_{0,n}, h_{1,n}, \cdots, h_{L_{\text{delay}}-1,n}]^{\mathsf{T}} \in \mathbb{C}^{L_{\text{delay}}}$ are the RS matrix, fast Fourier transform (FFT) matrix, and channel impulse response (CIR) vector at the angle θ_n. Thus, the frequency-domain signal vector received at the m-th antenna element $\mathbf{r}_m \in \mathbb{C}^{N_{\text{RS}}}$ is represented by

$$\begin{aligned}\mathbf{r}_m &= \sum_{n=0}^{N_{\text{bin}}-1} a_{n,m}\mathbf{XFh}_n + \mathbf{z}_m \\ &= \mathbf{XFHa}_m + \mathbf{z}_m, \end{aligned} \tag{1}$$

where $\mathbf{a}_m = [a_{0,m}, a_{1,m}, \cdots, a_{N_{\text{bin}}-1,m}]^{\mathsf{T}} \in \mathbb{C}^{N_{\text{bin}}}$ is the antenna pattern vector of the m-th antenna element, $\mathbf{H} = [\mathbf{h}_0, \mathbf{h}_1, \cdots, \mathbf{h}_{N_{\text{bin}}-1}] \in \mathbb{C}^{L_{\text{delay}} \times N_{\text{bin}}}$ is the CIR matrix, and $\mathbf{z}_m \in \mathbb{C}^{N_{\text{RS}}}$ is the noise vector. Here, the (p, l)-element of $\mathbf{F}$ is given by

$$f_{p,l} = \exp\left(-j\frac{2\pi k_p l}{N_F}\right), \tag{2}$$

where k_p is the subcarrier index of the p-th RS, and N_F is the number of FFT points. By using Eq. (1), the frequency-domain received signal matrix

$\mathbf{R} = [\mathbf{r}_0, \mathbf{r}_1, \cdots, \mathbf{r}_{M-1}] \in \mathbb{C}^{N_{\mathrm{RS}} \times M}$ is represented by

$$\mathbf{R} = \mathbf{XFHA} + \mathbf{Z}, \tag{3}$$

where $\mathbf{A} = [\mathbf{a}_0, \mathbf{a}_1, \cdots, \mathbf{a}_{M-1}] \in \mathbb{C}^{N_{\mathrm{bin}} \times M}$ and $\mathbf{Z} = [\mathbf{z}_0, \mathbf{z}_1, \cdots, \mathbf{z}_{M-1}] \in \mathbb{C}^{N_{\mathrm{RS}} \times M}$ are the antenna pattern matrix and noise matrix, respectively.

Assuming the uniform circular array (UCA) antenna [40], [41], which enables wide-range DOA estimation compared with the uniform linear array (ULA) antenna, the (n, m)-element of $\mathbf{A}$ is theoretically given by [41]

$$a_{n,m} = \sqrt{G_m(\theta_n)} \exp\left(j\frac{2\pi}{\lambda} \cdot R\cos\left(\frac{2\pi m}{M} - \theta_n\right)\right), \tag{4}$$

where $G_m(\theta_n)$, λ, and R are the radiation pattern of the m-th antenna element, wavelength, and radius of the UCA antenna; in the experimental evaluation of the following section, the measured values were used for the antenna pattern matrix $\mathbf{A}$.

Equation (3) can be written equivalently in vector form as follows:

$$\mathrm{vec}(\mathbf{R}) = \{\mathbf{A}^{\mathsf{T}} \otimes (\mathbf{XF})\}\,\mathrm{vec}(\mathbf{H}) + \mathrm{vec}(\mathbf{Z}). \tag{5}$$

The CIR vector $\mathrm{vec}(\mathbf{H})$ is generally sparse, and hence we can estimate it by applying the CS approach to the received signal vector $\mathrm{vec}(\mathbf{R})$ [38], [39], [40], [41]. However, in Eq. (5), the vector or matrix size becomes large due to the Kronecker product; the application of the well-known vector-based CS approach [38], [39], [40], [41] to Eq. (5) leads to a problem of huge computational complexity. Thus, we adopt the matrix-based CS approach, such as the matrix-based fast iterative shrinkage-thresholding algorithm (FISTA) [42], [48], to reduce computational complexity, and apply it directly to the matrix form of Eq. (3).

By using the matrix-based FISTA [42], [48], the CIR matrix is iteratively updated as follows:

$$\mathbf{H}^{(i)} = S_{\gamma/L_f}(\mathbf{W}^{(i)} + L_f^{-1}(\mathbf{XF})^{\mathsf{H}}(\mathbf{R} - \mathbf{XFW}^{(i)}\mathbf{A})\mathbf{A}^{\mathsf{H}}), \tag{6}$$

where i $(= 1, 2, \cdots)$ is the iteration index; L_f is a Lipschitz constant, which is given as $2 \cdot \lambda_{\max}(\{\mathbf{A}^{\mathsf{T}} \otimes (\mathbf{XF})\}^{\mathsf{H}}\{\mathbf{A}^{\mathsf{T}} \otimes (\mathbf{XF})\}) = 2 \cdot \lambda_{\max}((\mathbf{XF})^{\mathsf{H}}(\mathbf{XF})) \cdot \lambda_{\max}(\mathbf{AA}^{\mathsf{H}})$ [49]; γ is a regularization parameter that determines sparsity of the CIR matrix; $S.(\cdot)$ is the shrinkage thresholding function, which is defined as

$$[S_a(\mathbf{B})]_{i,j} = \begin{cases} \frac{|b_{i,j}| - a}{|b_{i,j}|} & a < |b_{i,j}| \\ 0 & \text{otherwise}, \end{cases} \tag{7}$$

where a and $\mathbf{B} = [b_{i,j}]$ are an arbitrary scalar and matrix, respectively. In Eq. (6), $\mathbf{W}^{(\cdot)}$ is calculated by

$$\mathbf{W}^{(i+1)} = \mathbf{H}^{(i)} + \frac{\beta^{(i)} - 1}{\beta^{(i+1)}}(\mathbf{H}^{(i)} - \mathbf{H}^{(i-1)}), \tag{8}$$

where $\beta^{(\cdot)}$ is represented by

$$\beta^{(i+1)} = \frac{1}{2} + \sqrt{\frac{1}{4} + (\beta^{(i)})^2}. \tag{9}$$

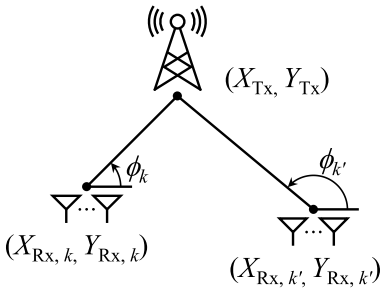

FIGURE 6. Concept of wave source location estimation.

The initial values of the iterative process in Eqs. (6)–(9) are set as follows:

$$\mathbf{H}^{(0)} = \mathbf{O}, \tag{10}$$

$$\mathbf{W}^{(1)} = \mathbf{O}, \tag{11}$$

$$\beta^{(1)} = 1. \tag{12}$$

For the CIR matrix obtained by Eqs. (6)–(9), the element with the highest power is considered as the LOS component. Therefore, the estimated DOA corresponding to such an element is used for the wave source location estimation.

D. WAVE SOURCE LOCATION ESTIMATION

Fig. 6 shows the concept of the wave source location estimation. As shown in Fig. 6, using DOAs ϕ_k and Rx locations $(X_{\mathrm{Rx},k}, Y_{\mathrm{Rx},k})$ $(k = 1, 2, \cdots, K)$, the Tx location $(X_{\mathrm{Tx}}, Y_{\mathrm{Tx}})$ is estimated based on the triangulation [50], [51], [52]. Since the estimated DOAs obtained by the method in Section III-C are relative values with respect to the Rx placement directions, and hence the absolute values of DOAs are calculated using the Rx orientations obtained by the GPS compass.

The relationship between the DOA and locations is represented by [50], [51], and [52]

$$\tan\phi_k = \frac{Y_{\mathrm{Tx}} - Y_{\mathrm{Rx},k}}{X_{\mathrm{Tx}} - X_{\mathrm{Rx},k}}. \tag{13}$$

By using both DOAs and locations of two Rx points #k and #k', the Tx location can be estimated as follows:

$$\hat{X}_{\mathrm{Tx},k,k'} = (X_{\mathrm{Rx},k}\tan\phi_k - X_{\mathrm{Rx},k'}\tan\phi_{k'} - Y_{\mathrm{Rx},k} + Y_{\mathrm{Rx},k'}) \times \frac{1}{\tan\phi_k - \tan\phi_{k'}}, \tag{14}$$

$$\hat{Y}_{\mathrm{Tx},k,k'} = \{(X_{\mathrm{Rx},k} - X_{\mathrm{Rx},k'})\tan\phi_k\tan\phi_{k'} - Y_{\mathrm{Rx},k}\tan\phi_{k'} + Y_{\mathrm{Rx},k'}\tan\phi_k\} \times \frac{1}{\tan\phi_k - \tan\phi_{k'}}. \tag{15}$$

Here, the Tx location can be calculated for each combination of two Rx points, and the mean operation is usually applied to them [52]. In practice, the DOAs and locations required for the triangulation have measurement errors [50], which leads to the degradation of the location estimation accuracy. Therefore, in order to mitigate such measurement errors, we apply the trimmed mean operation [53], [54], which calculates the

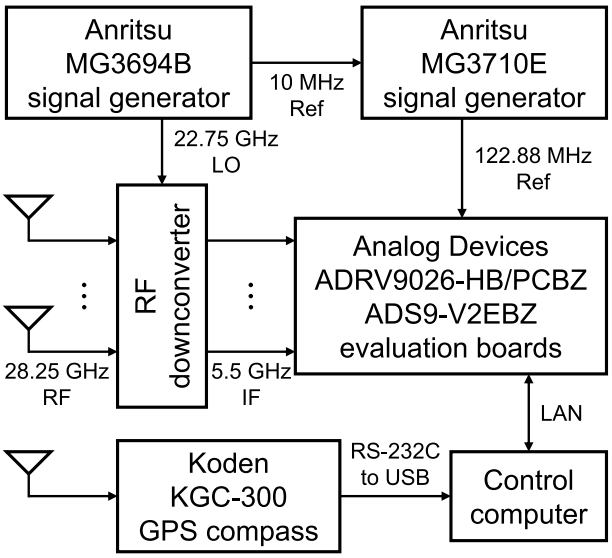

FIGURE 7. Configuration of our measurement system.

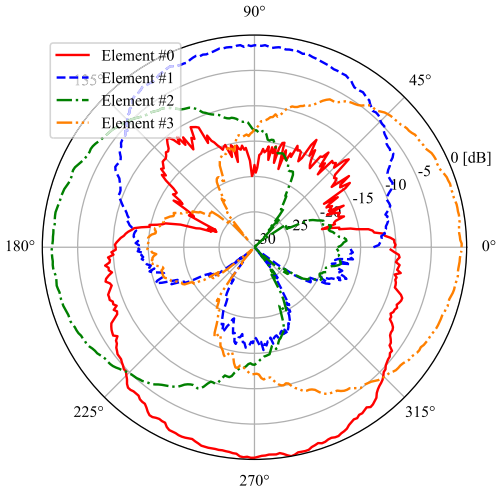

FIGURE 8. Antenna element radiation pattern in our measurement system.

mean after discarding the outliers, to Eqs. (14) and (15), and then the estimated Tx location $(\hat{X}_{\mathrm{Tx}}, \hat{Y}_{\mathrm{Tx}})$ is represented by

$$\hat{X}_{\mathrm{Tx}} = \frac{1}{N_{\mathrm{comb}} - 2\lceil \alpha N_{\mathrm{comb}} \rceil} \cdot \sum_{i=\lceil \alpha N_{\mathrm{comb}} \rceil + 1}^{N_{\mathrm{comb}} - \lceil \alpha N_{\mathrm{comb}} \rceil} \hat{X}_{\mathrm{Tx},(i)}, \quad (16)$$

$$\hat{Y}_{\mathrm{Tx}} = \frac{1}{N_{\mathrm{comb}} - 2\lceil \alpha N_{\mathrm{comb}} \rceil} \cdot \sum_{i=\lceil \alpha N_{\mathrm{comb}} \rceil + 1}^{N_{\mathrm{comb}} - \lceil \alpha N_{\mathrm{comb}} \rceil} \hat{Y}_{\mathrm{Tx},(i)}, \quad (17)$$

where $\lceil \cdot \rceil$ denotes the ceiling function, α is the trimming percentage, N_{comb} is the number of combinations of the two Rx locations, and $\hat{X}_{\mathrm{Tx},(i)}$ and $\hat{Y}_{\mathrm{Tx},(i)}$ are the i-th sorted values of $\hat{X}_{\mathrm{Tx},k,k'}$ and $\hat{Y}_{\mathrm{Tx},k,k'}$, respectively.

IV. EXPERIMENTAL RESULTS

A. MEASUREMENT SYSTEM

Fig. 7 shows the configuration of our measurement system. For the SS/PBCH block detection and CS-based DOA estimation, 28.25 GHz-band radio frequency (RF) signals were received by the array antenna and downconverted to 5.5 GHz intermediate frequency (IF) signals. The IF signals were then captured by Analog Devices ADRV9026-HB/PCBZ and ADS9-V2EBZ evaluation boards and baseband signal data with a sampling rate of $f_{\mathrm{sam}} = 245.76$ MHz was stored in storage on a control computer. Moreover, for the wave source location, the Rx locations and orientations were also acquired by Koden KGC-300 GPS compass.

The UCA antenna [40], [41] was adopted as the Rx array antenna. Fig. 8 shows the radiation pattern of the UCA antenna in our measurement system. The number of antenna elements was set to four, the element spacing was $1/2$ wavelength, and the beamwidth of each antenna element was 90 deg [41]. The number of bins N_{bin} and the width of each bin were set to 360 and 1 deg, respectively, and thus the DOA estimation range was $[0, 360)$ deg.

In the DOA estimation, the maximum delay time $\tau_{L_{\mathrm{delay}}-1}$ was set equal to the cyclic prefix (CP) duration [35], and the delay time resolution was $1/f_{\mathrm{sam}}$. The number of FFT points was calculated by $N_F = f_{\mathrm{sam}} \cdot T_s$, where T_s is the OFDM symbol duration, which is the inverse of the subcarrier spacing.

B. BASIC PERFORMANCE EVALUATION OF CS-BASED DOA ESTIMATION

In this section, we present the basic performance evaluation of the CS-based DOA estimation in our measurement system, prior to the wave source location estimation. According to the CS theory, the property of the sensing matrix determines the reconstruction accuracy of sparse signals, and smaller correlation coefficients calculated from its matrix lead to the better reconstruction performance [41], [45]. Thus, we first analyze the correlation coefficients in DOA and delay domains, respectively.

For the DOA domain, the reconstruction performance depends on the antenna pattern matrix $\mathbf{A}$ in Eq. (3), and the correlation coefficient $R_\theta(n, n')$ is calculated by [41]

$$R_\theta(n, n') = \frac{\sum_{m=0}^{M-1} a_{n,m}^* a_{n',m}}{\sqrt{\sum_{m=0}^{M-1} |a_{n,m}|^2} \sqrt{\sum_{m=0}^{M-1} |a_{n',m}|^2}}. \quad (18)$$

Similarly, for the delay domain, the matrix $\mathbf{XF}$ is considered to affect the reconstruction performance. Then, the correlation coefficient $R_\tau(l, l')$ is expressed as

$$R_\tau(l, l') = \frac{\sum_{p=0}^{N_{\mathrm{RS}}-1} (X_p f_{p,l})^* (X_p f_{p,l'})}{\sqrt{\sum_{p=0}^{N_{\mathrm{RS}}-1} |X_p f_{p,l}|^2} \sqrt{\sum_{p=0}^{N_{\mathrm{RS}}-1} |X_p f_{p,l'}|^2}}. \quad (19)$$

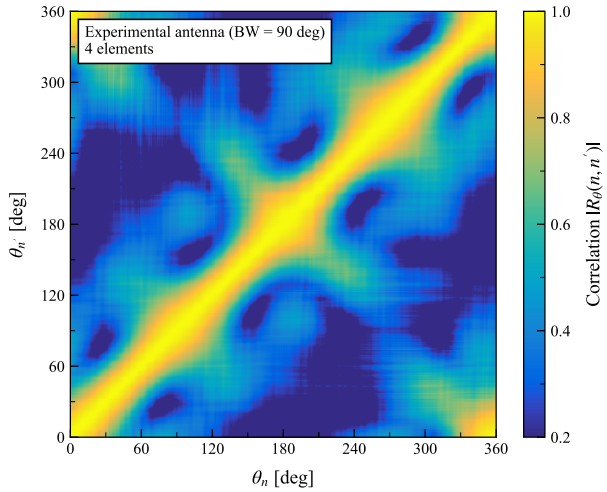

(a) Experimental antenna in our measurement system

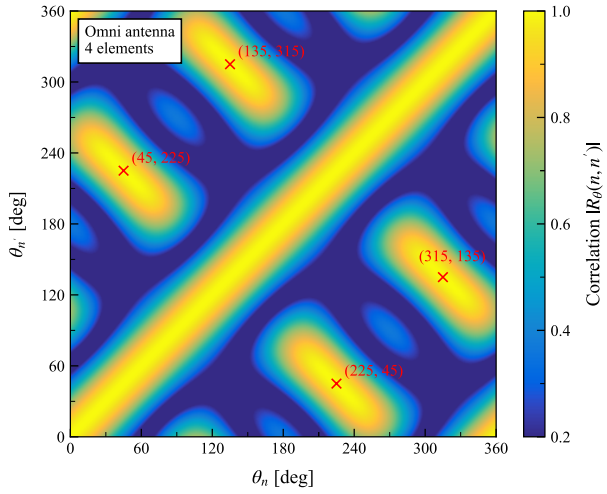

(b) Omni-directional antenna [41]

FIGURE 9. Correlation coefficient in DOA domain.

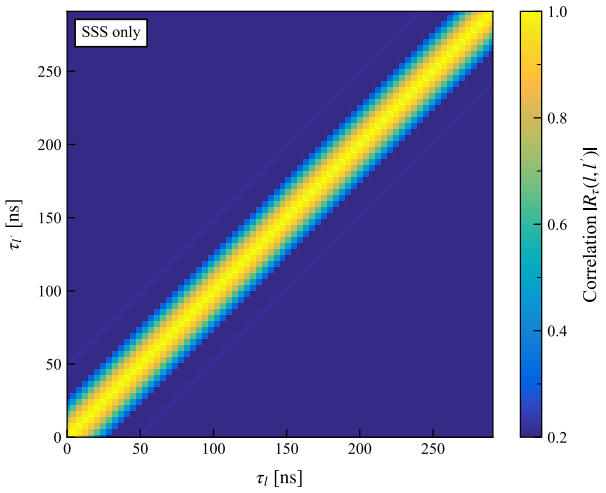

(a) SSS only (Case 1)

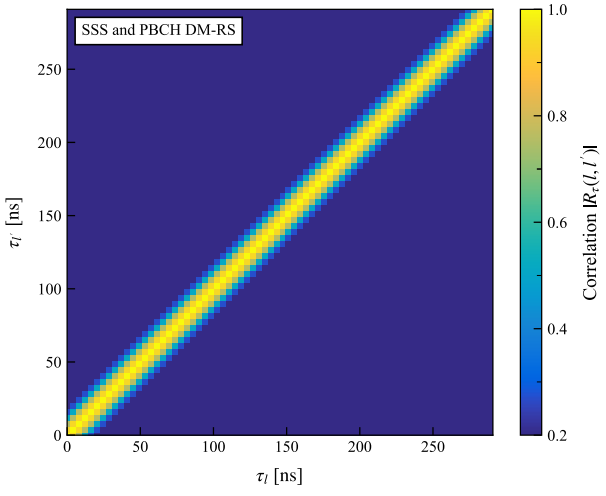

(b) SSS and PBCH DM-RS (Case 2)

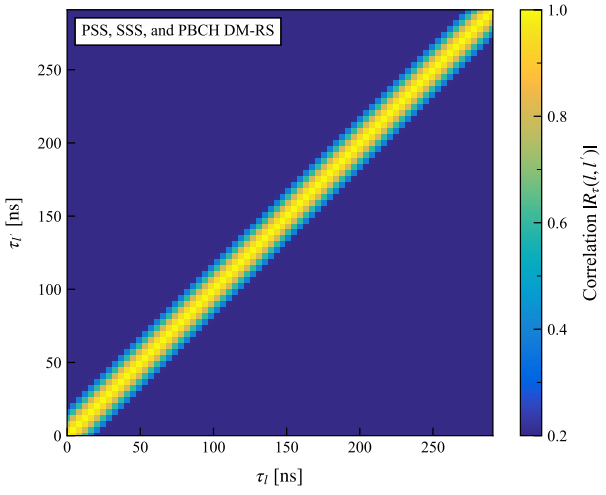

(c) PSS, SSS, and PBCH DM-RS (Case 3)

FIGURE 10. Correlation coefficient in delay domain.

Fig. 9 shows the correlation coefficient in the DOA domain. In Fig. 9(a), the correlation coefficient was obtained from the measured pattern of the experimental antenna of Fig. 8; in Fig. 9(b), the theoretical value was calculated, where the number of antenna elements, radiation pattern, and radius of the UCA antenna in Eq. (4) were set to $M = 4$, $G_m(\theta_n) = 1$, and $R = 0.5\lambda/\sqrt{2}$. It is observed from Fig. 9 that in the omni-directional antenna, the correlation coefficients between angle pairs of $(45, 225)$ deg and $(135, 315)$ deg become large, due to omni-directivity. This indicates that if the incident wave arrives at such angles, the estimation accuracy can be significantly degraded [41]. In contrast, the experimental antenna in our measurement system can reduce the correlation coefficients between such angle pairs, thanks to antenna directivity.

Fig. 10 shows the correlation coefficient in the delay domain, where the subcarrier spacing was set to 240 kHz. In Fig. 10, as the configuration of the RS in the matrix **XF**, we adopted SSS only (Case 1), SSS and PBCH DM-RS (Case 2), or PSS, SSS, and PBCH DM-RS (Case 3). It is found from Fig. 10 that the RS configuration in Case 2 provides the lower correlation compared to that in Case 1. This is

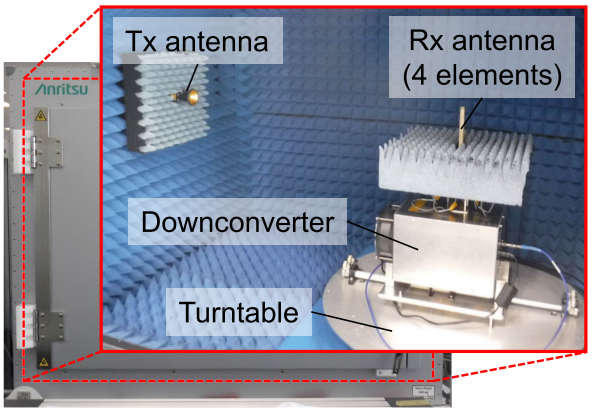

FIGURE 11. Setup for accuracy evaluation of CS-based DOA estimation in RF chamber.

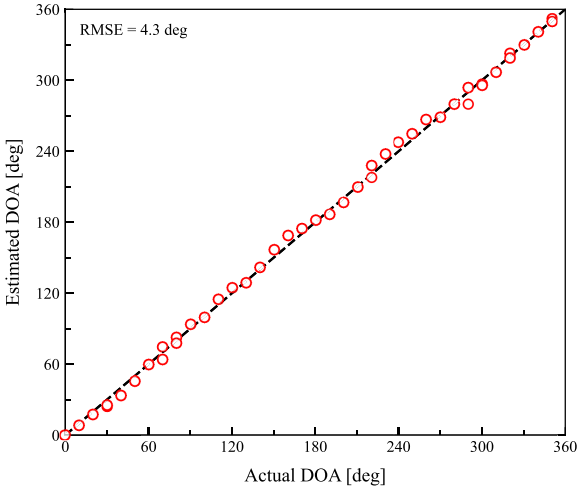

FIGURE 12. Estimated DOA versus actual DOA.

because the PBCH DM-RS is included in the RSs of Case 2, which has a wider bandwidth than the SSS. Moreover, even with the addition of the PSS, the correlation coefficients in Case 3 are almost the same as those in Case 2. Therefore, in the following, we adopt Case 2 as the RS configuration in the CS-based DOA estimation.

Next, we evaluate the CS-based DOA estimation accuracy of our measurement system. Fig. 11 shows the setup for the accuracy evaluation of the CS-based DOA estimation. We conducted the measurement experiment in Anritsu MA8171A RF chamber. At the transmitter, SS/PBCH blocks were generated by Rohde & Schwarz SMW200A vector signal generator and transmitted from a horn antenna. The Tx level, carrier frequency, and subcarrier spacing were set to -20 dBm, 28.25 GHz, and 240 kHz, respectively. At the receiver, the four-element UCA antenna with the downconverter was mounted on a turntable and rotated every 10 deg. The regularization parameter was chosen to be $\gamma = 3.0 \times 10^2$.

Fig. 12 shows the CS-based DOA estimation result over 50 trials per actual DOA, where the signal-to-noise

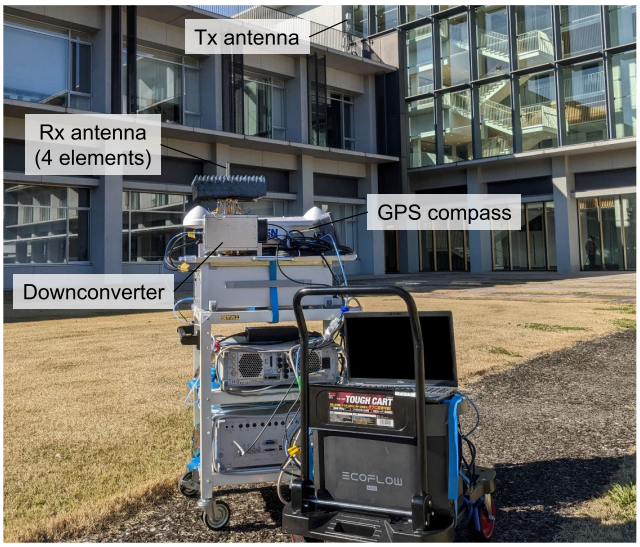

FIGURE 13. Setup for performance evaluation of wave source location estimation in outdoor environment.

ratios (SNRs) of the antenna elements #0, #1, #2, and #3 were 31.5, 31.1, 31.4, and 31.6 dB at the actual DOAs of 270, 90, 180, and 0 deg, respectively. In Fig. 12, the root-mean-square error (RMSE) is also presented, which is given by

$$\mathrm{RMSE} = \sqrt{\frac{1}{T}\sum_{t=1}^{T}(\hat{\theta}_t - \theta_t)^2}, \tag{20}$$

where T denotes the number of total trials, θ_t is the actual DOA, and $\hat{\theta}_t$ is the estimated DOA. It is found from Fig. 12 that our measurement system provides the relatively high estimation accuracy irrespective of the actual DOA and achieves the RMSE of 4.3 deg.

C. PERFORMANCE EVALUATION OF WAVE SOURCE LOCATION ESTIMATION IN OUTDOOR ENVIRONMENT

In this section, we evaluate the performance of the wave source location estimation. Fig. 13 shows the setup for the performance evaluation of the wave source location estimation in the outdoor environment. We performed measurements at 20 Rx points with communication distances between 20 m and 90 m in Hino Campus, Tokyo Metropolitan University, Japan. The zero degree angle of the UCA antenna in Fig. 8 was pointed north, at all 20 points. The carrier frequency and subcarrier spacing of Ericsson BS were 28.25004 GHz and 120 kHz, respectively. The heights of the Tx and Rx antennas were 12 m and 1.3 m, respectively. The regularization parameter was selected as $\gamma = 4.8 \times 10^2$.

Fig. 14 shows the SS-RSRP at each Rx point, where the boresight of the Tx antenna was pointed to Rx #13, and 12 SS/PBCH blocks with different indices were detected. In Fig. 14, a maximum value of the SS-RSRP among the four antenna elements is shown [46], [55]. It is observed that

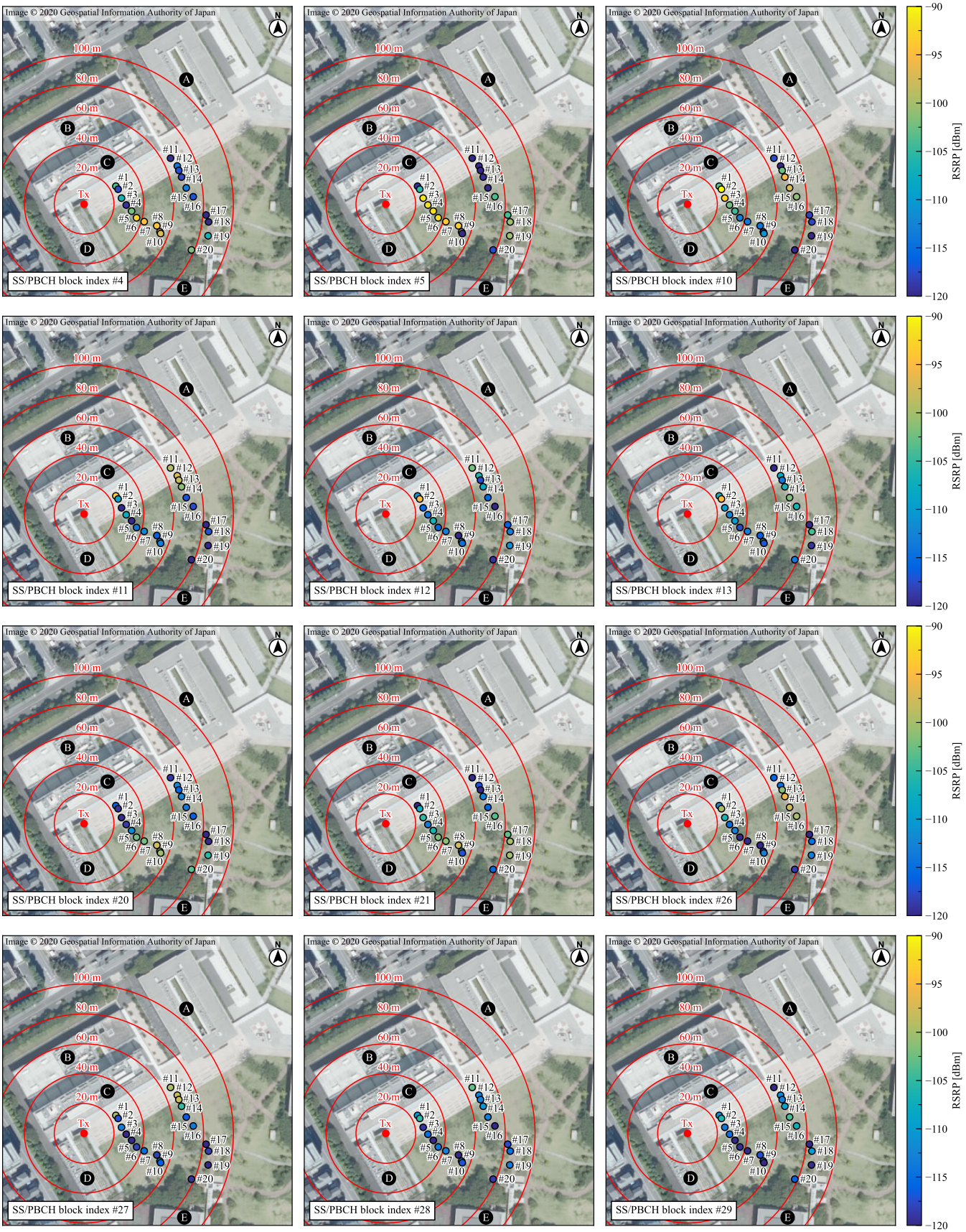

FIGURE 14. RSRP for each SS/PBCH block index.

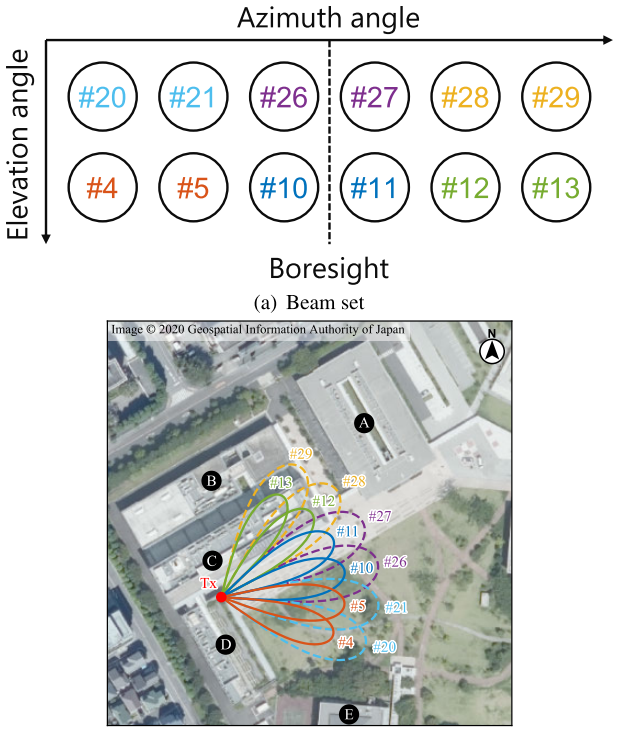

FIGURE 15. Transmit beams deduced from RSRPs.

the SS-RSRP varies significantly due to the different transmit beam patterns. Specifically, at Rx point #2, the SS-RSRP gap between SS/PBCH block indices #4 and #10 is a large value of 27 dB. This result implies the need to select a beam with high received power at each Rx point.

Here, we consider the transmit beams in more detail, because their information helps us to discuss the DOA estimation results. Unfortunately, however, the parameters of the transmit beams are confidential information of some BS vendors. Thus, we try to deduce the transmit beams from the RSRP measurements. From Fig. 14, the following can be seen:

- At Rx points #1–5 and #11–15, which are located directly in front of Tx antenna, RSRPs for SS/PBCH block indices #10, #11, #26, and #27 tend to be higher.
- At Rx points #6–10 and #16–20, which are located on the building E side, RSRPs for SS/PBCH block indices #4, #5, #20, and #21 tend to be higher.
- At Rx points #1–10, RSRPs for SS/PBCH block indices #4–13 tend to be higher; for SS/PBCH block indices #20–29, RSRPs are degraded.

Therefore, the transmit beam set can be derived as shown in Fig. 15(a), where the numbers correspond to the SS/PBCH block indices. Six and two beam patterns are assumed in the azimuth and elevation directions, respectively. Fig. 15(b) illustrates the deduced transmit beam patterns. It is noted that the pattern of each beam is imagined based on the above observation and may differ from the actual pattern.

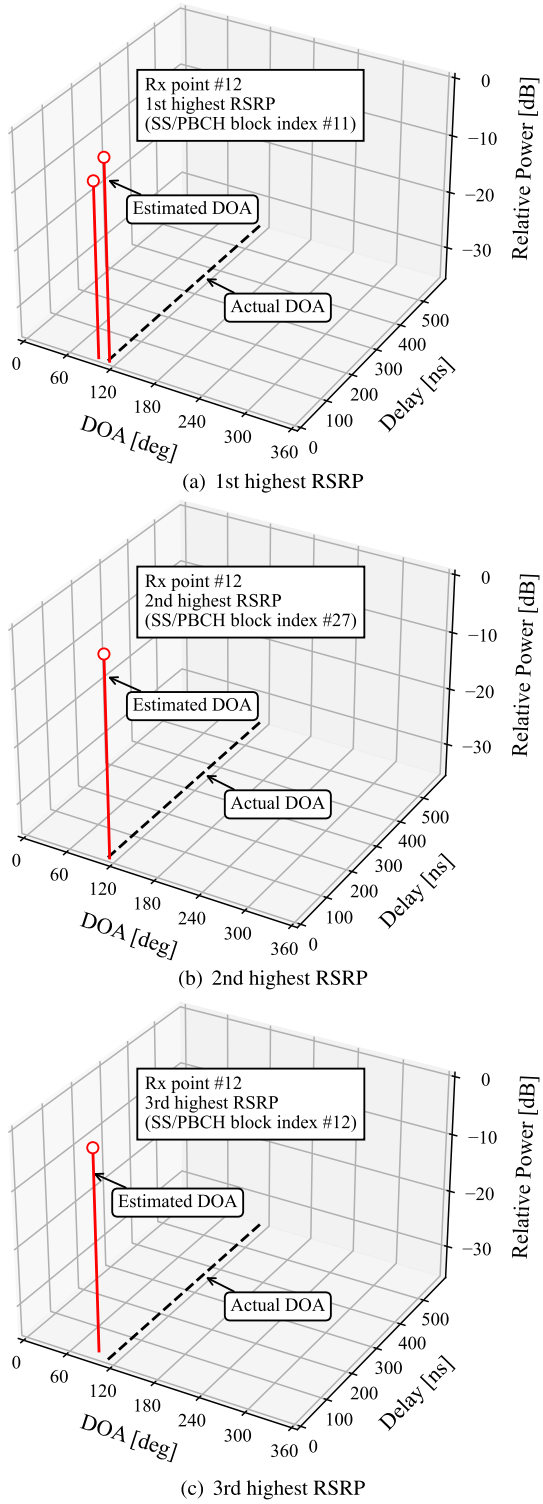

FIGURE 16. CS-based DOA estimation results at Rx point #12.

Fig. 16 shows the CS-based DOA estimation results for the top three SS/PBCH blocks with the highest SS-RSRP at Rx #12. In Fig. 16, the relative power corresponds to the power value of the element $h_{l,n}$ of the estimated CIR

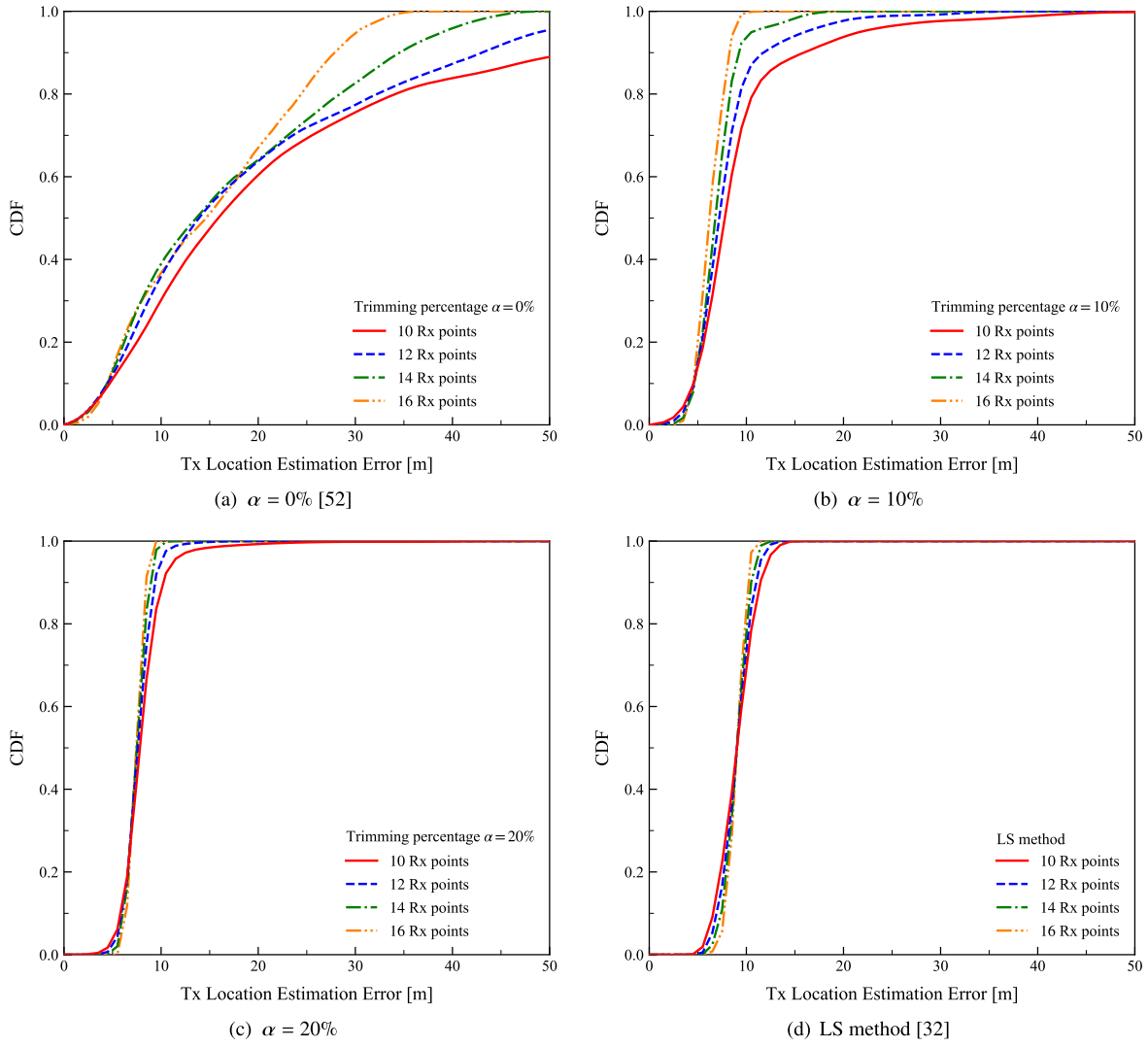

FIGURE 17. CDF of Tx location estimation error with a parameter of the number of Rx points.

matrix $\mathbf{H}$, and the actual DOA calculated from the actual Tx location and the GPS-compass-based Rx location and orientation is also shown for reference. It is found that in the case of the third highest RSRP, there is a difference between the estimated and actual DOAs. This is because the transmit beam for the SS/PBCH block index #12 is not aimed at the Rx, but at the building C, resulting that the impact of reflected wave becomes dominant. On the other hand, since the transmit beam for the SS/PBCH block index #11 or #27 is directed at the Rx, the CS-based DOA estimation provides almost the same value as the actual DOA in the first or second highest RSRP case.

Table 2 shows the wave source location estimation results based on the DOAs and Rx locations at the 20 points, with a parameter of the trimming percentage. Note that the number of combinations of the two Rx locations is calculated as $N_{\text{comb}} = 190$. Moreover, in Table 2, the estimation error of the least squares (LS) method [32] is also shown for reference. Here, the LS method estimates the Tx location as follows:

$$\begin{bmatrix} \hat{X}_{\text{Tx}} \\ \hat{Y}_{\text{Tx}} \end{bmatrix} = (\mathbf{G}^{\mathsf{T}}\mathbf{G})^{-1}\mathbf{G}^{\mathsf{T}} \begin{bmatrix} X_{\text{Rx},1}\sin\phi_1 - Y_{\text{Rx},1}\cos\phi_1 \\ X_{\text{Rx},2}\sin\phi_2 - Y_{\text{Rx},2}\cos\phi_2 \\ \vdots \\ X_{\text{Rx},K}\sin\phi_K - Y_{\text{Rx},K}\cos\phi_K \end{bmatrix}, \tag{21}$$

TABLE 2. Tx location estimation error with 20 Rx points.

Trimming percentage α	Tx location estimation error
0% [52]	13.9 m
10%	5.8 m
20%	7.9 m
30%	8.2 m
LS method [32]	9.5 m

$$\mathbf{G} = \begin{bmatrix} \sin\phi_1 & -\cos\phi_1 \\ \sin\phi_2 & -\cos\phi_2 \\ \vdots & \vdots \\ \sin\phi_K & -\cos\phi_K \end{bmatrix}. \tag{22}$$

It can be seen that in the traditional case without trimming [52], such as $\alpha = 0\%$, the Tx location estimation error is as poor as 13.9 m. In detail, the triangulation of Eqs. (14) and (15) results in the worst error of 1409 m for the combination of the Rx points #4 and #7, and such an outlier due to measurement errors significantly degrades the accuracy of the Tx location estimation. However, it is observed that the trimmed mean operation improves the estimation accuracy owing to the exclusion of outliers. In particular, the 10% trimmed mean achieves the better estimation error of 5.8 m, compared with the LS method [32]. This is because although the LS method is designed to minimize the Tx location estimation error under the assumption of the error-free DOA estimation, in practice, the accuracy of the location estimation is degraded due to the DOA estimation error. Moreover, it is found that too large a trimming percentage deteriorates the Tx location estimation error, because some relatively accurate estimates are also discarded along with the outliers.

Finally, we evaluate the impact of the number of Rx points on the accuracy of the wave source location estimation. In this evaluation, 10, 12, 14, or 16 Rx points were randomly selected from 20 Rx points, and then the source location estimation was conducted based on these Rx points. Fig. 17 shows the cumulative distribution function (CDF) of the Tx location estimation error, where the trimming percentages $\alpha = 0\%$ [52], 10%, and 20%. In Fig. 17, the CDF of the least squares (LS) method [32] is also shown for reference, and $N_{\text{comb}} = 45$, 66, 91, and 120 for 10, 12, 14, and 16 Rx points, respectively. It is found that an increase in the number of Rx points reduces the estimation error. Specifically, when $\alpha = 0\%$ and 10%, the Tx location estimation errors based on 10 Rx points are 52.9 and 16.4 m, respectively, at the 90th percentile; in the case of 16 Rx points, 28.4 and 8.7 m, respectively, are achived. Furthermore, it is observed that the estimation accuracy is improved owing to the trimmed mean operation, regardless of the number of Rx points. In particular, the trimming percentage $\alpha = 20\%$ provides the Tx location estimation errors of 10.6 and 8.9 m at the 90th percentile from 10 and 16 Rx points, respectively, which are sperior to 11.9 and 10.6 m in the LS method [32].

V. CONCLUSION

In this paper, we experimentally investigated a DOA-based wave source location estimation method for spectrum sharing in millimeter-wave band local and private 5G systems. In the DOA-based wave source location estimation, it is important to extract a LOS component from the received signals. Considering that SS/PBCH blocks for the initial access are transmitted with beam-sweeping in 5G systems, our measurement system performed the DOA estimation based on the maximum-power block. In the DOA estimation, taking advantage of the sparsity of the propagation channels in both angular space and delay time domains, our measurement system adopted the CS-based approach. Experimental results showed that the received power varies significantly due to the different transmit beam patterns and that the extraction of the LOS component by beam selection improves the accuracy of the DOA estimation. Moreover, our measurement system achieves the location estimation error of 5.8 m based on 20 measurements with the four-element UCA antenna.

Although the CS-based approach was adopted for the DOA estimation herein, in practice, the estimated DOA is constrained to the fixed grid due to the discrete signal modeling [56], [57], i.e., Eq. (3). This grid mismatching problem can lead to a degradation in the accuracy of the wave source location estimation. In our future work, we will further consider the mitigation of this problem.

ACKNOWLEDGMENT

The authors would like to thank Keisuke Takizawa, Hideki Fujishima, Takeshi Kobayashi, and Ikuya Otani for their continuing support.

REFERENCES

[1] *Ericsson Mobility Report*. Accessed: Nov. 2022. [Online]. Available: https://www.ericsson.com/4ae28d/assets/local/reports-papers/mobility-report/documents/2022/ericsson-mobility-report-november-2022.pdf

[2] S. Chen, Y. Liang, S. Sun, S. Kang, W. Cheng, and M. Peng, "Vision, requirements, and technology trend of 6G: How to tackle the challenges of system coverage, capacity, user data-rate and movement speed," *IEEE Wireless Commun.*, vol. 27, no. 2, pp. 218–228, Apr. 2020.

[3] *Study on Scenarios and Requirements for Next Generation Access Technologies*, document TR 38.913, V14.2.0, 3GPP, Mar. 2017.

[4] M. Shafi, A. F. Molisch, P. J. Smith, T. Haustein, P. Zhu, P. De Silva, F. Tufvesson, A. Benjebbour, and G. Wunder, "5G: A tutorial overview of standards, trials, challenges, deployment, and practice," *IEEE J. Sel. Areas Commun.*, vol. 35, no. 6, pp. 1201–1221, Jun. 2017.

[5] A. Aijaz, "Private 5G: The future of industrial wireless," *IEEE Ind. Electron. Mag.*, vol. 14, no. 4, pp. 136–145, Dec. 2020.

[6] M. Wen, Q. Li, K. J. Kim, D. López-Pérez, O. A. Dobre, H. V. Poor, P. Popovski, and T. A. Tsiftsis, "Private 5G networks: Concepts, architectures, and research landscape," *IEEE J. Sel. Topics Signal Process.*, vol. 16, no. 1, pp. 7–25, Jan. 2022.

[7] *System Architecture for the 5G System (5GS); Stage 2*, document TS 23.501, V16.5.0, 3GPP, Jul. 2020.

[8] Y. Siriwardhana, P. Porambage, M. Ylianttila, and M. Liyanage, "Performance analysis of local 5G operator architectures for industrial internet," *IEEE Internet Things J.*, vol. 7, no. 12, pp. 11559–11575, Dec. 2020.

[9] J. Prados-Garzon, P. Ameigeiras, J. Ordonez-Lucena, P. Muñoz, O. Adamuz-Hinojosa, and D. Camps-Mur, "5G non-public networks: Standardization, architectures and challenges," *IEEE Access*, vol. 9, pp. 153893–153908, 2021.

[10] N. Ul Hasan, W. Ejaz, N. Ejaz, H. S. Kim, A. Anpalagan, and M. Jo, "Network selection and channel allocation for spectrum sharing in 5G heterogeneous networks," *IEEE Access*, vol. 4, pp. 980–992, 2016.

[11] H. Gao, W. Ejaz, and M. Jo, "Cooperative wireless energy harvesting and spectrum sharing in 5G networks," *IEEE Access*, vol. 4, pp. 3647–3658, 2016.

[12] Y. Wu, B. Li, S. Liu, and X. Wang, "Spectrum sharing between radar and communication systems based on overlapped virtual subarrays," *IEEE Access*, vol. 10, pp. 94841–94850, 2022.

[13] M. Matinmikko-Blue, S. Yrjölä, V. Seppänen, P. Ahokangas, H. Hämmäinen, and M. Latva-Aho, "Analysis of spectrum valuation approaches: The viewpoint of local 5G networks in shared spectrum bands," in *Proc. IEEE Int. Symp. Dyn. Spectr. Access Netw. (DySPAN)*, Oct. 2018, pp. 1–9.

[14] H. Nakajo, Y. Aoki, K. Katagiri, and T. Fujii, "High density spectrum sharing method among micro operators considering spectrum database," in *Proc. IEEE Wireless Commun. Netw. Conf. Workshop (WCNCW)*, Apr. 2019, pp. 1–5.

[15] A. Haniz, T. Matsumura, and F. Kojima, "Efficient joint sensing of sparse angular-frequency spectrum based on compressive sensing," in *Proc. IEEE 31st Annu. Int. Symp. Pers., Indoor Mobile Radio Commun.*, Aug. 2020, pp. 1–7.

[16] S. Tomida, K. Mizutani, and H. Harada, "Radio protection area estimation methods for spectrum sharing-based 5G system," in *Proc. IEEE 18th Annu. Consum. Commun. Netw. Conf. (CCNC)*, Jan. 2021, pp. 1–4.

[17] A. Karstensen, T. Kolding, C. Rosa, L. G. Uzeda Garcia, K. I. Pedersen, and N. Hathiramani, "Spectrum for private networks: Challenges and opportunities—A case study based on Danish regulation," *IEEE Access*, vol. 10, pp. 69346–69353, 2022.

[18] P. Hanpinitsak, K. Murakami, J. Takada, and K. Saito, "Maximum-likelihood-based location, orientation, transmitted power, and antenna beamwidth estimator utilizing the angle-of-arrival and received power for spectrum sharing at millimeter wave bands," *IEEE Access*, vol. 11, pp. 6896–6911, 2023.

[19] K. S. V. Prasad and V. K. Bhargava, "RSS-based positioning in distributed massive MIMO under unknown transmit power and pathloss exponent," in *Proc. IEEE 90th Veh. Technol. Conf. (VTC-Fall)*, Sep. 2019, pp. 1–5.

[20] H. Matsuno, Y. Kunisawa, and T. Hayashi, "Location estimation algorithm for multiple wave sources using power gravity points," in *Proc. 23rd Int. Symp. Wireless Pers. Multimedia Commun. (WPMC)*, Oct. 2020, pp. 1–6.

[21] C. Zhan, M. Ghaderibaneh, P. Sahu, and H. Gupta, "DeepMTL pro: Deep learning based multiple transmitter localization and power estimation," *Pervas. Mobile Comput.*, vol. 82, Jun. 2022, Art. no. 101582.

[22] L. Hao, B. Huang, B. Jia, and G. Mao, "DHCLoc: A device-heterogeneity-tolerant and channel-adaptive passive WiFi localization method based on DNN," *IEEE Internet Things J.*, vol. 9, no. 7, pp. 4863–4874, Apr. 2022.

[23] Y. Zhao, N. Cheng, Z. Li, and B. Hao, "An efficient sensor selection algorithm for TDOA localization with estimated source position," in *Proc. IEEE Int. Conf. Commun.*, May 2022, pp. 871–876.

[24] G. Torsoli, M. Z. Win, and A. Conti, "Selection of reference base station for TDOA-based localization in 5G and beyond IIoT," in *Proc. IEEE Globecom Workshops (GC Wkshps)*, Dec. 2022, pp. 317–322.

[25] Y. Liu, Z. Gong, Z. Zhang, L. Wu, R. Gui, J. Dang, and B. Zhu, "High-precision single base station localization assisted by beamforming," in *Proc. 2nd Inf. Commun. Technol. Conf. (ICTC)*, pp. 178–183, May 2021.

[26] B. Hu, Y. Wang, and Z. Shi, "Simultaneous position and reflector estimation (SPRE) by single base-station," in *Proc. IEEE Wireless Commun. Netw. Conf. (WCNC)*, Apr. 2018, pp. 1–6.

[27] H. Lim, K. Lim, I. Joo, J.-B. Kim, and S.-U. Lee, "Experimental performance of signal source localization based on distributed DoA measurements," in *Proc. 34th Int. Tech. Conf. Circuits/Syst., Comput. Commun.*, Jan. 2019, pp. 1–3.

[28] D. He, X. Chen, L. Pei, F. Zhu, L. Jiang, and W. Yu, "Multi-BS spatial spectrum fusion for 2-D DOA estimation and localization using UCA in massive MIMO system," *IEEE Trans. Instrum. Meas.*, vol. 70, pp. 1–13, 2021.

[29] S. Takase, K. Nishimori, R. Taniguchi, T. Matsuda, and T. Mitsui, "Source location estimation via compressed sensing using UAVs," in *Proc. Int. Symp. Antennas Propag. (ISAP)*, Jan. 2021, pp. 237–238.

[30] H. Takarada, K. Nishimori, S. Takase, and T. Matsuda, "Experimental evaluation of a wave source location estimation method using UAVs," in *Proc. Int. Symp. Antennas Propag. (ISAP)*, Oct. 2021, pp. 1–2.

[31] P. Hanpinitsak, K. Murakami, K. Saito, and J. Takada, "Angle-of-arrival-based outdoor localization for spectrum sharing at 25 GHz band," in *Proc. Int. Symp. Antennas Propag.*, Jan. 2021, pp. 745–746.

[32] H. El-Sayed, G. Athanasiou, and C. Fischione, "Evaluation of localization methods in millimeter-wave wireless systems," in *Proc. IEEE 19th Int. Workshop Comput. Aided Model. Design Commun. Links Netw. (CAMAD)*, Dec. 2014, pp. 345–349.

[33] J. Talvitie, T. Levanen, M. Koivisto, T. Ihalainen, K. Pajukoski, M. Renfors, and M. Valkama, "Positioning and location-based beamforming for high speed trains in 5G NR networks," in *Proc. IEEE Globecom Workshops*, Dec. 2018, pp. 1–7.

[34] D. Kurita, D. Kitayama, K. Miyachi, Y. Kishiyama, S. Itoh, H. Murai, A. Simonsson, P. Ökvist, J.-K. Fwu, X. Zhuang, and K. Stewart, "Outdoor experiments on 5G radio access in 5G trial site using core network in 28-GHz frequency band," in *Proc. IEEE 90th Veh. Technol. Conf.*, Sep. 2019, pp. 1–6.

[35] *NR; Physical Channels and Modulation*, document TS 38.211, V15.2.0, 3GPP, Jun. 2018.

[36] *NR; Physical Layer Procedures for Control*, document TS 38.213, V15.2.0, 3GPP, Jun. 2018.

[37] A. Chakrapani, "On the design details of SS/PBCH, signal generation and PRACH in 5G-NR," *IEEE Access*, vol. 8, pp. 136617–136637, 2020.

[38] D. L. Donoho, M. Elad, and V. N. Temlyakov, "Stable recovery of sparse overcomplete representations in the presence of noise," *IEEE Trans. Inf. Theory*, vol. 52, no. 1, pp. 6–18, Jan. 2006.

[39] J. W. Choi, B. Shim, Y. Ding, B. Rao, and D. I. Kim, "Compressed sensing for wireless communications: Useful tips and tricks," *IEEE Commun. Surveys Tuts.*, vol. 19, no. 3, pp. 1527–1550, 3rd Quart., 2017.

[40] S. Uemura, K. Nishimori, R. Taniguchi, M. Inomata, K. Kitao, T. Imai, S. Suyama, H. Ishikawa, and Y. Oda, "Direction-of-arrival estimation with circular array using compressed sensing in 20 GHz band," *IEEE Antennas Wireless Propag. Lett.*, vol. 20, no. 5, pp. 703–707, May 2021.

[41] H. Suganuma, K. Takizawa, T. Kobayashi, I. Otani, and T. Mitsui, "Impact of antenna directivity on compressed sensing-based DOA estimation employing UCA antenna," *IEICE Commun. Exp.*, vol. 12, no. 4, pp. 132–138, Apr. 2023.

[42] K. Shimoshige, K. Tategami, and M. Fujimoto, "Acceleration of DOA-TOA simultaneous estimation by matrix based compressed sensing with zero bin removal," in *Proc. Int. Symp. Antennas Propag. (ISAP)*, Jan. 2021, pp. 605–606.

[43] M. Wu and C. Hao, "Super-resolution TOA and AOA estimation for OFDM radar systems based on compressed sensing," *IEEE Trans. Aerosp. Electron. Syst.*, vol. 58, no. 6, pp. 5730–5740, Dec. 2022.

[44] W. Wei, R. Liu, X. Yu, Q. Lu, G. Cui, X. Fang, and L. Zhang, "DOA estimation of distributed mmWave radar system via fast iterative adaptive approach," in *Proc. Int. Conf. Control, Autom. Inf. Sci. (ICCAIS)*, Oct. 2021, pp. 414–418.

[45] M. Lin, M. Xu, X. Wan, H. Liu, Z. Wu, J. Liu, B. Deng, D. Guan, and S. Zha, "Single sensor to estimate DOA with programmable metasurface," *IEEE Internet Things J.*, vol. 8, no. 12, pp. 10187–10197, Jun. 2021.

[46] *NR; Physical Layer Measurements*, document TS 38.215, V15.2.0, 3GPP, Jun. 2018.

[47] F. Gomez-Cuba and A. J. Goldsmith, "Sparse mmWave OFDM channel estimation using compressed sensing," in *Proc. IEEE Int. Conf. Commun. (ICC)*, Shanghai, China, May 2019, pp. 1–7.

[48] T. Wimalajeewa, Y. C. Eldar, and P. K. Varshney, "Recovery of sparse matrices via matrix sketching," 2013, *arXiv:1311.2448*.

[49] B. Liu, Y. Zhao, X. Zhu, S. Matsushita, and L. Xu, "Sparse detection algorithms based on two-dimensional compressive sensing for sub-Nyquist pulse Doppler radar systems," *IEEE Access*, vol. 7, pp. 18649–18661, 2019.

[50] L. A. Martínez Hernández, S. Pérez Arteaga, G. Sánchez Pérez, A. L. Sandoval Orozco, and L. J. García Villalba, "Outdoor location of mobile devices using trilateration algorithms for emergency services," *IEEE Access*, vol. 7, pp. 52052–52059, 2019.

[51] W. Shieh, Y. Zhang, C. Hsu, and X. Guo, "A study of error reduction in optical triangulation for short-range intervehicle positioning," *IEEE Photon. J.*, vol. 14, no. 2, pp. 1–12, Apr. 2022.

[52] Y. Tian, S. Liu, W. Liu, H. Chen, and Z. Dong, "Vehicle positioning with deep-learning-based direction-of-arrival estimation of incoherently distributed sources," *IEEE Internet Things J.*, vol. 9, no. 20, pp. 20083–20095, Oct. 2022.

[53] P. J. Huber, *Robust Statistics*. Hoboken, NJ, USA: Wiley, 1981.

[54] J. Bednar and T. Watt, "Alpha-trimmed means and their relationship to median filters," *IEEE Trans. Acoust., Speech, Signal Process.*, vol. ASSP-32, no. 1, pp. 145–153, Feb. 1984.

[55] *Impact of Receiver Diversity on RSRP Measurement Accuracy*, R4-090290, Ericsson, Stockholm, Sweden, Jan. 2009.
[56] Y. Chi, L. L. Scharf, A. Pezeshki, and A. R. Calderbank, "Sensitivity to basis mismatch in compressed sensing," *IEEE Trans. Signal Process.*, vol. 59, no. 5, pp. 2182–2195, May 2011.
[57] Z. Yang, L. Xie, and C. Zhang, "Off-grid direction of arrival estimation using sparse Bayesian inference," *IEEE Trans. Signal Process.*, vol. 61, no. 1, pp. 38–43, Jan. 2013.

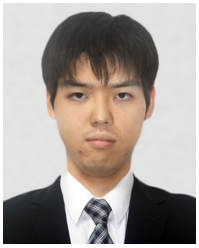

HIROFUMI SUGANUMA (Member, IEEE) received the B.Eng., M.Eng., and D.Eng. degrees from Waseda University, Tokyo, Japan, in 2016, 2018, and 2020, respectively. From 2020 to 2021, he was an Assistant Professor with the School of Fundamental Science and Engineering, Waseda University. Since 2022, he has been engaged in the research and development of test and measurement systems with Anritsu Corporation, Kanagawa, Japan. His current research interest includes mobile communication systems. He is a member of IEICE.

TSUTOMU MITSUI received the B.E. degree from the Musashi Institute of Technology, Tokyo, Japan, in 1987, and the Ph.D. degree from the University of Niigata Prefecture, Japan, in 2017. In 1987, he joined Tokyo Keiki Inc., Japan. In 1999, he joined Samsung Yokohama Research Institute Corporation, Kanagawa, Japan. In 2016, he joined Koden Electronics Corporation, Tokyo. He was a Research Fellow with the Nippon Institute of Technology, Japan, from 2017 to 2020. Since 2021, he has been with Anritsu Corporation, Kanagawa. His research interests include antenna systems and propagation. He is a member of the IEICE.

TAKAHIRO MATSUDA (Member, IEEE) received the B.E. (Hons.), M.E., and Ph.D. degrees in communications engineering from Osaka University, in 1996, 1997, and 1999, respectively. In 1999, he joined the Department of Communications Engineering, Graduate School of Engineering, Osaka University, where he was an Assistant Professor, from 1999 to 2005, a Lecturer, from 2005 to 2009, and an Associate Professor, from 2009 to 2018. He is currently a Professor with the Department of Computer Science, Graduate School of Systems Design, Tokyo Metropolitan University. His research interests include performance analysis and the design of communication networks and wireless communications. He is a member of IPSJ and a Senior Member of IEICE. He received the Best Tutorial Paper Award and the Best Magazine Paper Award from IEICE ComSoc, in 2012, and the Best Paper Award from IEICE, in 2014.